ARMY RESEARCH LABORATORY

Self-Propagating High-Temperature Synthesis and Dynamic Compaction of Titanium Boride and Titanium Carbide

by Liya Wang and Levi T. Thompson

ARL-CR-440 April 1999

prepared by

T/J Technologies, Inc.
3850 Research Park Drive
P.O. Box 2150
Ann Arbor, MI 48106

under contract

DAAA-15-91-C-0088

The findings in this report are not to be construed as an official Department of the Army position unless so designated by other authorized documents.

Citation of manufacturer's or trade names does not constitute an official endorsement or approval of the use thereof.

Destroy this report when it is no longer needed. Do not return it to the originator.

Army Research Laboratory
Aberdeen Proving Ground, MD 21005-5066

ARL-CR-440 **April 1999**

Self-Propagating High-Temperature Synthesis and Dynamic Compaction of Titanium Boride and Titanium Carbide

Liya Wang and Levi T. Thompson
T/J Technologies, Inc.

prepared by

T/J Technologies, Inc.
3850 Research Park Drive
P.O. Box 2150
Ann Arbor, MI 48106

under contract

DAAA-15-91-C-0088

Abstract

Titanium carbide (TiC) and titanium diboride (TiB_2) ceramic disks, with diameters of 100 mm and thicknesses of 25 mm, were fabricated with densities above 95% and 98% of theoretical, respectively, using a self-propagating high-temperature synthesis/dynamic consolidation (SHS/DC) process. First, an SHS reaction was initiated in a green body made from precursor powders. Second, after the completion of the SHS reaction, the freshly synthesized ceramic product was densified to near-full density by the action of the detonation of an explosive. With a focus on potential military and civilian applications, the structural and mechanical properties of the products were evaluated. Furthermore, the relationship between process conditions, microstructure development, and mechanical properties was investigated. Finally, correlations of the properties with key processing conditions were used to establish guidelines for the fabrication, scale-up, and commercialization of the process.

Table of Contents

List of Figures

INTENTIONALLY LEFT BLANK.

List of Tables

INTENTIONALLY LEFT BLANK.

1. Introduction

There is great interest in the development of light armor for improving the performance of armored vehicles and for using in some domestic applications. The major requirements for an armor material include high compressive strength, high elastic impedance, and low specific gravity [1, 2]. Titanium diboride (TiB_2) and titanium carbide (TiC) possess these characteristics and are ideal candidates for applications in armor. In addition, they are refractory (melting points for TiB_2 and TiC are 2,980° C and 3,067° C, respectively), ultrahard (hardnesses for TiB_2 and TiC are 3,400 kg/mm^2 and 3,200 kg/mm^2, respectively), wear resistant, thermal shock resistant, chemically stable, and lightweight (densities of TiB_2 and TiC are 4.571 kg/cm^3 and 4.911 kg/cm^3, respectively) [3–5]. These properties make TiB_2 and TiC attractive for other applications, including use in cutting tools, wear-resistant components, rocket nozzles, and jet engine components.

The fabrication of TiB_2 and TiC ceramics by conventional sintering, hot-pressing, or hot-isostatic pressing (HIPing) of TiB_2 and TiC powders is costly because of the time-intensive and facility-intensive nature of these processes. The application of TiB_2 and TiC ceramics has thus been limited. The development of the self-propagating high-temperature synthesis (SHS) technique, however, may provide an economical method for producing TiB_2 and TiC ceramics. The SHS process takes advantage of the extreme heat generated during the formation of some refractory materials. When a mixture of the constituent elements is ignited at one end, the highly exothermic reaction propagates spontaneously and rapidly and converts the reactants into a refractory product. The reaction temperature can exceed 2,500° C. The SHS technique has attracted attention as a route to a variety of refractory materials, including borides, carbides, nitrides, silicides, and intermetallic compounds [6–21].

The SHS products cannot be used directly as structural materials because they are generally quite porous (the porosity can be as high as 50 volume-percent). This porosity can be reduced by compressing the SHS product while it remains at a temperature above its ductile-brittle transition point. A number of methods that combine a compaction step with the SHS process have been

developed in order to exploit the high post-reaction temperature. Among these are SHS/hot-pressing [22, 23], SHS/HIPing [24, 25], SHS/hot-forging [26, 27], SHS/hot-rolling [28], and SHS/dynamic compaction (DC) [29–32]. These methods hold promise for the economical synthesis of armor materials due to their low costs and high productivity, as compared to hot-pressing and HIPing. While the costs of products generated using the SHS-based techniques are yet to be compared, the SHS/DC method is the least facility-intensive and time-intensive process. This technique has been employed for the synthesis of TiB_2, TiC and hafnium carbide (HfC) by scientists at the U.S. Army Ballistic Research Laboratory (BRL)* [29–31, 33–37].

2. Literature Survey

While the SHS technique was developed more than a century ago, it did not receive much attention until the mid-1960s, when Merzhanov [38, 39] (in the former Soviet Union) used this technique to produce powders of refractory compounds. Today, the total number of materials that can be prepared by this technique exceeds 500, covering a wide range of materials, including carbides, borides, nitrides, silicides, and intermetallic compounds [6–37]. This progress has generated a great deal of interest around the world, and a number of research efforts have been initiated in the U.S. and Japan in the past few years.

Advantages of the SHS process are as follows [11, 13]: (1) the materials are usually purer because the extremely high reaction temperatures cause the expulsion of volatile contaminates and no catalysts or other compounds are involved, (2) this process has a high energy efficiency since no heat is needed except for the ignition, (3) the process has the potential for high production efficiencies due to the very quick processing times (on the order of seconds instead of hours and days for competing techniques), (4) the capital investment is low compared to conventional techniques, and (5) it is possible to produce metastable materials due to the fast cooling rates. Materials prepared by the SHS process can easily be crushed to form powders; however, they

*BRL was deactivated on 30 September 1992 and subsequently became a part of the U.S. Army Research Laboratory (ARL) on 1 October 1992.

cannot be used directly as structural materials because of their high porosity (as high as 50%). The porosity is caused by several factors, including the violent expulsion of volatile contaminants, the original porosity in the greenforms, and the molar volume difference between the reactants and products [40].

In order to make dense bodies, the SHS prepared materials must be further processed. There are a number of processes that combine SHS with a densification step. These processes include the following [11]: (1) simultaneous synthesis and sintering of the product, (2) use of a liquid phase in the SHS process to bind the products together and form a dense body, and (3) application of pressure during or shortly after the synthesis reaction to density the products.

Two primary reasons have limited the use of the first method. First, the SHS reaction time is too short to achieve sufficient sintering. Second, the expulsion of volatile impurities often causes swelling of the products. Prolonged post-sintering of the SHS-prepared materials may not be effective because of the high porosity after the SHS reaction. There are also several problems associated with the second method. While generation of a liquid phase may lead to effective sintering and the production of certain composites or compounds [41, 42], it may not be suitable for making monolithic compounds with very high melting points like TiB_2 and TiC. In addition, shrinkage of the liquid during the rapid cooling could limit the densification.

The last process is based on the concept that, while the temperature of the SHS product is still above the brittle-ductile transition point, it can easily be compacted by applying a force. This method has recently received a great deal of attention because of its ability to achieve synthesis and compaction in a short time. The following describes several approaches that have been developed.

- Hot-Pressing - Mixed powders are placed into a die and ignited. A uniaxial pressure is applied during or shortly after the reaction to compact the hot reaction products into dense ceramic bodies [22, 23].

- HIPing - The reactant mixture is vacuum-sealed in a glass envelope. The envelope is then embedded in a combustion reagent in a crucible. The assembly is placed inside a high-pressure vessel. When the combustion reagent is ignited, the heat generated sets off the reaction of the powder mixture inside the envelope. During the process, an isostatic pressure, which mechanically compacts the sample into a dense body, is maintained [24, 25].

- Hot-Forging - The SHS reaction is combined with a forging process so that the hot porous reaction products are forged into dense ceramics immediately after the reaction [26, 27].

- Hot-Rolling - Mixed reactants encased in insulated tubes are ignited and continuously compacted in a rolling mill immediately following passage of the reaction front [28].

- DC - Hot porous ceramic bodies formed during the SHS reactions are consolidated to high density by the action of a pressure wave from the detonation of a high explosive or impact of an explosively driven flyer plate [29–32].

While the costs and structural properties of the products prepared by these methods have not been compared, the DC technique has the merit of being less dependent on expensive facilities and higher in productivity. This method has been extensively studied by Niiler and coworkers at BRL [29–31]. They have demonstrated that, under the appropriate conditions, near fully dense TiB_2, TiC, and HfC ceramics could be prepared by this technique. Their work has also provided insight into the SHS/DC process. Valuable information regarding the effects of the powder characteristics, inert diluent, impurities, delay time, and (ratio of the explosive charge [C] mass to the metal driving plate mass [M]) on the synthesis and compaction was obtained. The results suggested that a pure starting powder; an appropriate delay time and C/M ratio; and a fixture, including a strong container and a thermal insulator with outgasing vent holes, were essential for the successful synthesis and consolidation of TiB_2 and TiC. The microhardness and ballistic performance of SHS/DC-prepared TiB_2 and TiC were comparable to those of the hot-pressed materials.

Thadhani and coworkers at the Center for Explosives Research and Technology at New Mexico Tech, continued the SHS/DC effort [32, 43, 44], based on results reported by Niiler and coworkers [29–31]. They modified the explosive loading assembly to obtain a more uniform compression of the samples. Dense TiB_2 (98% of theoretical) and TiC (95%) compacts were synthesized. Additional understanding of the process was obtained through both experiments and theoretical modeling.

T/J Technology, Inc., in response to a solicitation from the U.S. Department of Defense (DOD), completed a Phase I small business innovative research (SBIR) contract aimed at synthesizing near fully dense TiB_2 and TiC plates. This information is used to determine the feasibility of developing a commercial process based on the SHS/DC technique. The results are presented in this final report.

3. Technical Objectives

The primary objective of this project was to use the SHS/DC technique to fabricate 100-mm-diameter by 25-mm-thick plates of TiB_2 and TiC with densities greater than 98% and 95% of their theoretical values, respectively. The secondary objective was to evaluate the structural and mechanical properties of the synthesized TiB_2 and TiC and assess the feasibility of applying these ceramics in military and civilian uses. Finally, a desire existed to investigate the relationship between the processing conditions, microstructure development, and mechanical properties of TiB_2 and TiC. Of particular interest was the effect of precursor powder purity on the mechanical properties because pure boron (B) is very expensive. Correlations of the properties with the processing conditions provide guidelines for scaling-up and commercializing this process.

4. Experimental

4.1 Raw Materials. The starting materials were elemental powders of titanium (Ti), carbon (C), and B. The purity, particle size, and suppliers of the powders are summarized in

Table 1. Two different B powders were used. The B-1 powder contained 1–5% C, whereas the B-2 powder was ultrapure. The particle sizes were selected as a compromise between the reduced reaction rate of larger particles and the inconvenience of handling smaller particles [30].

Table 1. Specifications of the Starting Materials

Material	Purity (%)	Particle Size	Supplier
Ti	99.5	-325 mesh	Micron Metals
B-1	>95	-325 mesh	Aldrich
B-2	99.5	-325 mesh	Atlantic
C	99.9	2 μm	Consolidated Astronautics

4.2 Mixing and Greenform Preparation. The B/Ti atomic ratio of 2:1 and C/Ti atomic ratio of 0.95:1 were selected based on reports in the literature. A stoichiometric ratio of B/Ti has been widely used, whereas a range of C/Ti atomic ratios have been employed (0.7–1.19) [9, 29, 30, 40]. Several researchers have reported that the optimum C/Ti atomic ratio is 0.95 for SHS/DC [40, 45]. There are at least two reasons for the use of substoichiometric C/Ti ratios [27]. First, the violent release of impurities can cause expulsion of Ti from the compact [34]. Second, at the elevated temperatures at which compaction occurs, nonstoichiometric TiC has a lower yield strength than stoichiometric TiC [46].

The Ti-B and Ti-C powders were dry-mixed under an argon (Ar) atmosphere for 12 hr in a V-shaped plastic mechanical blender. Since no milling media was used, the possibility of contamination during mixing was minimal. The mixtures were uniaxially pressed into disk-shaped greenforms (100 mm in diameter with 40 mm thickness) using a hydraulic press. The greenforms were stored in a vacuum chamber to prevent oxidation.

4.3 SHS Reaction and DC. The experimental setup for the SHS/DC is shown in Figure 1. This is a modified version of the BRL design [30, 32, 40]. The system was made up of layers of gypsum wallboard, which were center-cored to a diameter slightly larger than that of the reactant

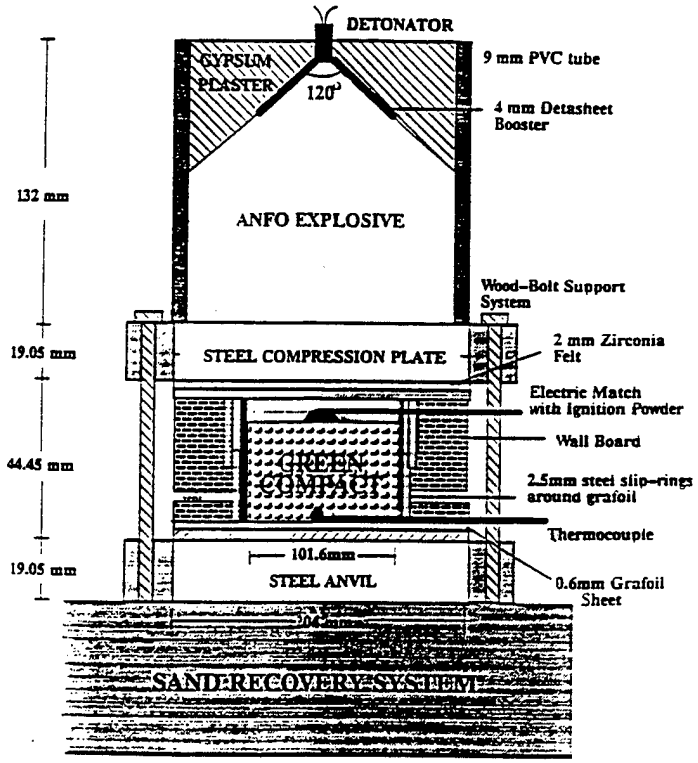

Figure 1. Experimental Setup for the SHS Reaction and DC.

greenforms. Two telescoping, mild steel rings of equal height were placed between the greenform and the gypsum to serve as lateral containment during the reaction and subsequent compaction. The bottom ring and the gypsum block had four matching holes to vent gases released during the reaction. A Grafoil strip was placed between the steel ring and the greenform to provide thermal insulation and prevent impurities from diffusing into the reacted compact. Circular driver plates and momentum traps made of high-hardness steel [47] were epoxied into wooden frames and lined with zirconia felt and a Grafoil sheet.

The explosive loading assembly consisted of a poly vinyl chloride (PVC) tube into which a 120° gypsum cone was cast. The apex of the cone was lined with a Detasheet booster and filled with ammonium nitrate mixed with 6-weight-percent fuel oil (ANFO) explosive with a density of 0.9 g/cm^3 and detonation velocity of 3,480 m/s. Such a cone-initiated explosive charge assembly provided a much more uniform pressure loading in comparison to that generated using sweeping-wave initiation of the explosive charge [32, 40].

Loose powder of the same composition as that of the reactant mixture was placed on the top of the greenform. The powder was ignited by an electric match using a 115-V source; this, in turn, set off the reaction between Ti and B or Ti and C in the greenform. The combustion wave traveled down toward the bottom surface of the greenform, and the completion of the reaction was verified using a chromel-alumel thermocouple attached to the surface of the momentum trap. Time to detonation (time delay between reaction completion and explosive compaction) was varied in an attempt to enhance the densities of the compacts. The same experimental setup was used for the synthesis of both TiB_2 and TiC.

The experimental conditions employed for the Ti-B and Ti-C systems are summarized in Table 2. The fixture used for the Ti-B system was 200 mm in diameter, whereas both 200-mm and 300-mm fixtures were used for the Ti-C system. Both the C/M ratio and delay time had significant influences on the product quality. The C/M ratio reflects the pressure applied to the samples during the explosion. While a low C/M ratio might not generate a pressure sufficient to fully compact the sample, a high C/M ratio could cause severe cracks and delamination in the sample due to strong rarefaction forces and edge effects from the shock waves. The C/M ratio suggested in reports by Niiler et al. [30] was 0.22 for the Ti-B system and 0.44 for the Ti-C system. The difficulty of compacting TiC compared to TiB_2 is reflected in the higher C/M ratio. Since the compressive yield strength at 1,800° C is 50 MPa for TiC [46] and 441 MPa for TiB_2 [48], a mechanism other than plastic deformation was probably involved. It has been postulated by Niiler et al. [30] that the melting point of TiB_2 was exceeded during the SHS process, whereas that of TiC was not. This implies that TiB_2 can be compacted more easily than TiC during SHS/DC because of the presence of some liquid phase. A C/M ratio of 0.2 was used for the Ti-B system, and two C/M ratios, 0.4 and 0.6, were used for the Ti-C system in this research.

The delay time influences the temperature at which the sample is compacted. A longer delay time usually means a lower temperature. If the delay time is too long, the compaction of the sample would be difficult due to the lack of plasticity at low temperatures. If, however, the delay time is too short, delamination of the sample could occur due to the after-burn phenomenon, leading to a

Table 2. Experimental Conditions for the SHS/DC of TiB_2 and TiC

Sample	Composition	C/M Ratio	Time Delay (s)	Fixture (mm)	Remarks
TB9224	B/Ti = 2:1	0.2	10	200	B-1
TB9225	B/Ti = 2:1	0.2	5	200	B-1
TB9244	B/Ti = 2:1	0.2	10	200	B-2
TB9245	B/Ti = 2:1	0.2	15	200	B-2
TB9246	B/Ti = 2:1	0.2	20	200	B-2
TC9223	C/Ti = 0.95:1	0.6	5	200	—
TC9241	C/Ti = 0.95:1	0.4	5	200	—
TC9242	C/Ti = 0.95:1	0.4	10	300	—
TC9243	C/Ti = 0.95:1	0.6	5	300	—

low density [32]. The optimum delay time depends on the system. Generally, the higher the reaction temperature, the longer the optimal delay time. The delay time was varied from 5 to 20 s in the present experiments.

4.4 Characterization. Samples for analysis were cut using a diamond saw from four areas within the compacts to examine the uniformity of the microstructural and mechanical properties. A schematic illustrating the locations of the four areas from which specimens were taken is given in Figure 2. Three specimens were taken from the center of the compact at varying distances from the impact surface compact top (CT), compact center (CC), and compact bottom (CB). Another specimen was taken from the area halfway between the compact center and the edge, middle center (MC). These specimens permitted an assessment of the transverse and radial uniformity.

4.4.1 Density. Density was measured for specimens cut from the central region using the Archimedes water displacement technique. The specimens were boiled in water for at least 2 hr to ensure that all open pores were filled with water. The displacement of water by each specimen was used to calculate the volume of the specimen. The density of stoichiometric TiB_2 (4.57 kg/cm^3) and that of $TiC_{0.9}$ (4.88 kg/cm^3) [27] were used to calculate the relative densities of the TiB_2 and TiC samples, respectively.

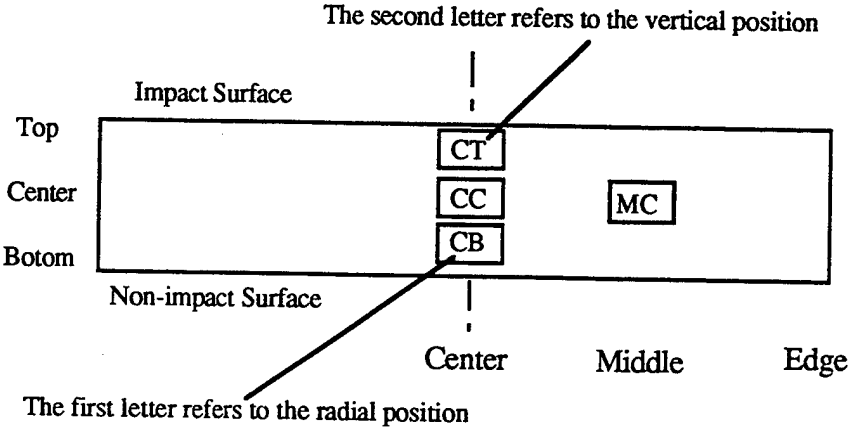

Figure 2. Illustration of Four Major Areas From Which Samples Were Obtained to Evaluate the Uniformity in Microstructure and Properties.

The pore sizes of selected samples were analyzed using a Micromeritics Model 9310 pore sizer. Mercury porosimetry is based on the capillary law governing liquid penetration into small pores. This law, in the case of nonwetting liquids like mercury and cylindrical pores, is expressed by the following equation [49],

$$d = -(1/p)4\gamma\cos\theta \quad , \tag{1}$$

where d is the pore diameter, p is the applied pressure, γ is the surface tension (485 dyn/cm), and θ is the contact angle (130°).

4.4.2 Composition. Phase constituents in the SHS reacted, and explosively densified compacts were determined by x-ray diffraction (XRD) using a Rigaku diffractometer. An energy-dispersive spectrometer attached to a Hitachi S-800 scanning electron microscope (SEM) was used to qualitatively analyze the composition of each phase, especially that of any secondary phases or impurities. The compositions of selected phases were quantitatively analyzed by electron microprobe analysis using a low-Z window detector capable of detecting B and C. The Ti content in each phase was assayed against a pure Ti standard. The B/Ti and C/Ti atomic ratios were calculated by assuming that the only other element was B in the TiB_2 grains and C in the TiC grains.

4.4.3 Microstructure. Specimens were polished sequentially using diamond pastes with grit sizes of 45, 30, 15, 6, and 1 μm. The polished samples were etched prior to microstructural analysis using a solution of two parts HNO_3, one part CH_3COOH, and one part HF. The microstructure was examined using an SEM. Grain sizes were determined from the SEM micrographs using the linear intercept technique developed by Mendelson [50], according to the following equation:

$$D = 1.57\ C/(NM), \tag{2}$$

where D is the grain size, C is the length of the test line, M is the magnification of the micrograph, and N is the number of grain boundary intercepts. The proportionality constant relates the grain size to the intercept length of a random section though a space-filling array of grains. At least four micrographs were taken from each area in the compact. Ten lines were drawn randomly on each micrograph. The average grain size was obtained from over 40 line measurements, which included several hundred grains and therefore provided a statistically reliable value.

4.4.4 Microhardness. Microhardness was measured by the Knoop indentation technique with a load of 0.1 kg. The hardness tests were performed on the specimens from all four areas in the compact. Between 20 and 30 indentations were made in each area to obtain a statistically significant result. The effect of grain boundary strength on hardness was examined by increasing the load to 5 and 10 kg.

4.4.5 Young's Modulus. The Young's moduli of selected materials were measured based on the velocity of sound through the specimens. The device used for the measurements consisted of a pulse circuit, transducer, and oscilloscope. A trigger generator in the system activated an electric switch, which produced large amplitude pulses. These pulses were applied to a transducer, which converted them into short ultrasonic pulses. The pulse wave bounced back and forth within the specimen. Each of the reflections was received by the transducer, and a train of echoes could be observed on the oscilloscope. The velocity of sound in the specimen was obtained by dividing

twice the thickness of the specimen by the time between two successive reflections. The Young's modulus, E, was calculated using the following equation [51]:

$$E = \rho \upsilon^2 , \qquad (3)$$

where ρ is the density of the specimen and υ is the sound velocity in the specimen.

4.4.6 Compressive Strength. The compressive strength of selected samples was measured using an INSTRON system. The specimens, with dimensions of $3.6 \times 3.6 \times 7.2$ mm, were prepared using a surface grinder. The two ends of the specimens were carefully ground so that they were parallel to each other. Two larger blocks of the same material were used as spacers between the rams and the test bar. A spherical seat was used to ensure good alignment.

5. Results and Discussion

5.1 TiB_2.

5.1.1 Physical Appearance of Compacts. The SHS reacted and explosively compressed compacts were usually recovered as single piece plates 100 mm in diameter with 25 mm thickness. A photograph of the impact surface of TB9225 is shown in Figure 3(a). The surface was smooth. The steel ring maintained its shape with no signs of melting or failure. No major cracks were observed, but some edge delamination occurred. For some samples synthesized from the ultrapure B-2 powder (like TB9246, which is shown in Figure 3[b]), the surfaces were much rougher and the steel rings were distorted or partially melted. Severe cracks were observed in these samples.

The results indicated the effect of the powder composition on the synthesis and consolidation of the samples. The TB9244 sample was synthesized using the same processing condition as those used for TB9224 except that the former used the B-2 powder rather than the B-1 powder. The TB9244 sample showed severe cracks and was blown into pieces. This might be related to the

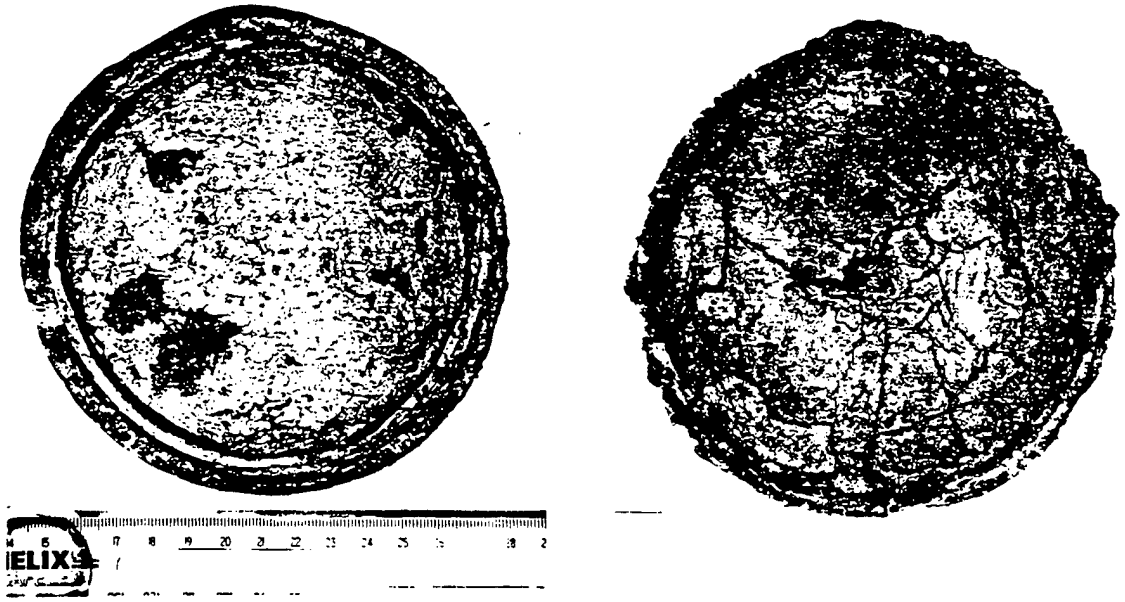

(a) TB9225. (b) TB9246.

Figure 3. Photographs of the TiB_2 Samples Showing Impact Surfaces.

different reactivities and, hence, different temperatures generated using the two powders. Since the heat of reaction is lower for TiC, C in the B-1 powder may have acted as a diluent and reduced the violence of the reaction. A 5-s delay time seemed adequate for successful compaction of the samples when using the B-1 powder. For the samples prepared using the B-2 powder, a 15-s delay time yielded the best results. A shorter (TB9244) or longer (TB9246) delay time caused severe cracks.

5.1.2 Density. The density, grain size, hardness, Young's modulus, and compressive strength of the TiB_2 samples are presented in Table 3. The relative density of TB9225 was 99.3% of the theoretical density. This result indicated that it was not necessary to use ultrapure B powders to achieve high density. The target density for TiB_2 in this Phase I project was 98% of the theoretical density. The lowest density was obtained for TB9246 (<85% of the theoretical density). While the diminished density for TB9246 compared to the other specimens may have been a consequence of using the purer B powder (a more violent reaction and failure of the steel containment), it is believed that the primary reason was that the delay time (20 s) was too long, resulting in sample compaction at a relatively low temperature.

Table 3. Density, Grain Size, Hardness, Young's Modulus, and Compressive Strength of SHS/DC TiB_2

Sample	Relative Density (%)	Grain Size[a] (μm)	Hardness[a] (kg/mm^2)	Young's Modulus (GPa)	Compressive Strength (GPa)
TB9224	97.2	CT: 20 ± 4	CT: 3351 ± 443	548 ± 18	1.8 ± 0.5
		CC: 19 ± 4	CC: 3291 ± 310	—	—
		CB: 16 ± 3	CB: 3309 ± 274	—	—
		MC: 17 ± 3	MC: 3193 ± 375	—	—
TB9225	99.3	CT: 18 ± 4	CT: 3356 ± 438	—	—
		CC: 18 ± 3	CC: 3387 ± 405	—	—
		CB: 17 ± 4	CB: 3354 ± 431	—	—
		MC: 17 ± 4	MC: 3265 ± 349	—	—
TB9246	84.6	CT: 23 ± 4	CT: 3273 ± 610	—	—
		CC: 29 ± 5	CC: 3277 ± 393	—	—
		CB: 29 ± 7	CB: 3297 ± 385	—	—
		MC: 30 ± 9	MC: 3213 ± 474	—	—

[a] CT, CC, CB, and MC refer to the positions illustrated in Figure 2.

A comparison of the experimental results for TB9224 and TB9225 clearly demonstrated the effect of delay time on the synthesis and compaction. The higher density for TB9225 relative to TB9224 was probably due to compaction of the former, while the sample was at a higher temperature (a shorter delay time), thus enhancing the densification through plastic deformation.

The density measured by the Archimedes immersion technique for TB9225 was further confirmed by a porosity measurement, which showed a porosity of 0.4 volume-percent. The results of mercury porosimetry analysis are shown in Figure 4. The total pore volume was 0.0008 cm^3/g, with 1-, 4-, 12-, and 93-μm-pore diameters, each accounting for 25% of the total pore volume.

5.1.3 Composition. XRD indicated that TB9225 consisted primarily of TiB_2, with a small amount of TiC (Figure 5[a]). There was no evidence of residual elemental Ti or B, indicating that the synthesis reaction proceeded to completion. The TiC was the result of C impurity in the precursor B powder (recall that B-1 contained 1–5% C). Electron microprobe analysis of the TiB_2

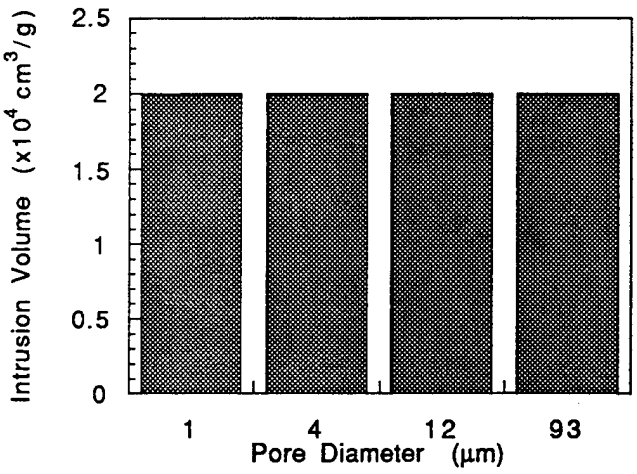

Figure 4. Intrusion Volume Against Pore Diameter for TB9225 Determined by Mercury Porosimetry Analysis.

grains showed that the B/Ti atomic ratio was 1.75. This corresponds to a B atomic fraction of 0.64, which is within experimental error of the lower limit of the stoichiometric range for TiB_2 (0.65), as given in the Ti-B phase diagram [52].

The XRD pattern of TB9246 is shown in Figure 5(b). Again, TiB_2 was the major phase, with TiC being a minor constituent. The TiC content in TB9246 was much lower than that in the samples prepared using the B-1 powder. One of the peaks in the diffraction pattern has been attributed to titanium carbonitride (TiCN). The formation of TiCN is possible because TiC and titanium nitride (TiN) can form an infinite solid solution.

5.1.4 Microstructure and Grain Size. Figure 6 shows an SEM micrograph of TB9225, the densest TiB_2 produced in this research. It shows a microstructure relatively free of porosity. This observation further supported the density and porosity measurements. It should be pointed out that pores larger than 10 μm were not observed by microscopy. The "large pores" revealed by mercury porosimetry might actually be cracks in the sample. This would explain the absence of evidence of large pores in the micrographs.

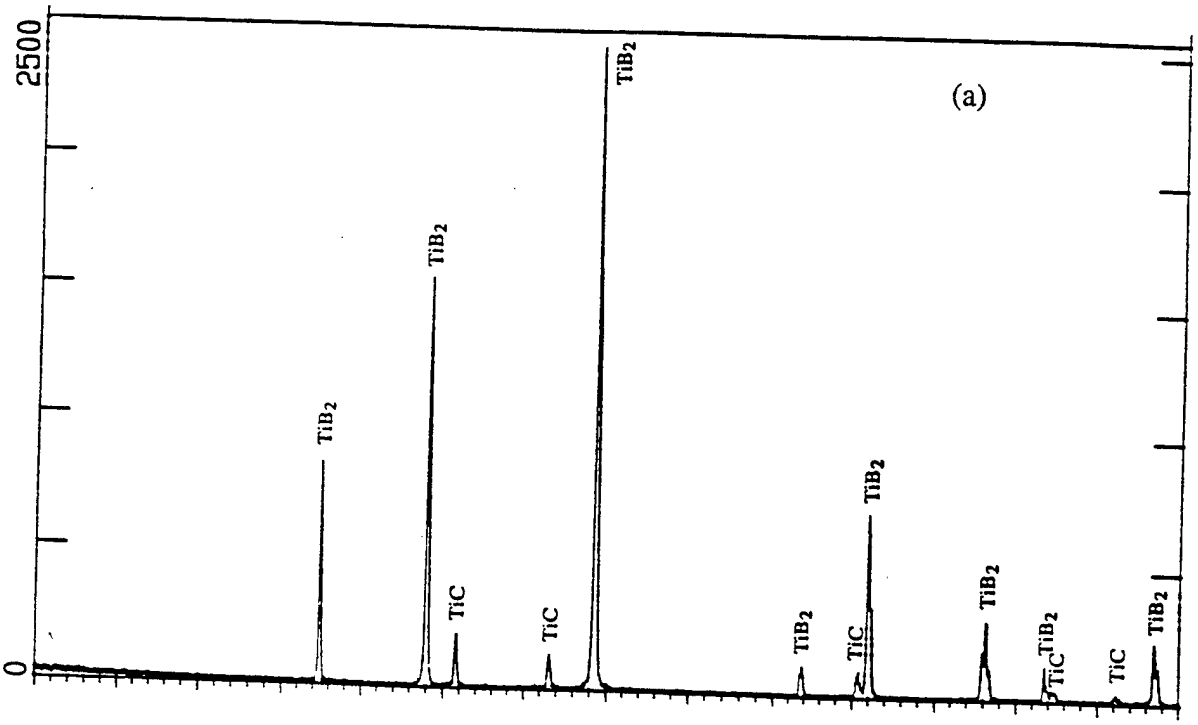

(a) TB9225.

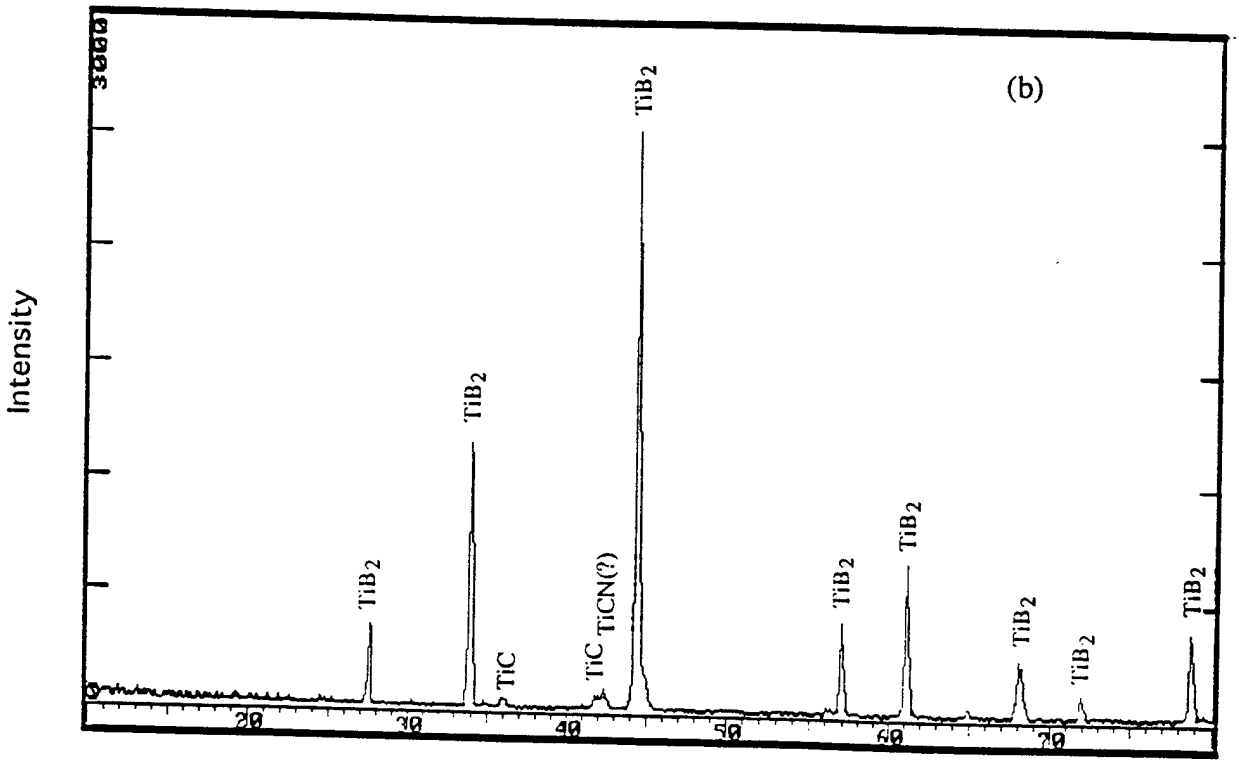

(b) TB9246.

Figure 5. XRD Patterns.

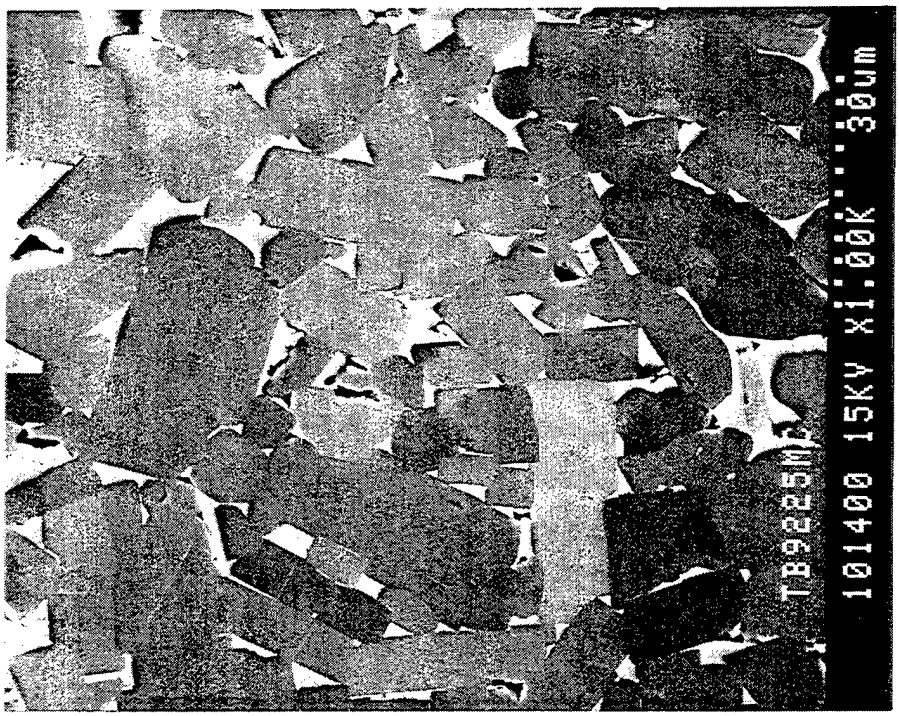

Figure 6. An SEM of TB9225.

The dark phase in the micrograph was due to TiB_2 grains with shapes that were consistent with a section cut through randomly oriented hexagonal single crystals. This supported the postulation that the melting point of TiB_2 was exceeded during the synthesis since single-crystal formation could only occur during cool-down from a liquid phase [30].

The light gray phase in Figure 6 was identified as TiC with a C/Ti atomic ratio of 0.80 by electron microprobe analysis. Some small but very bright white phases were also observed. These were found, by energy dispersive spectrum analysis, to be an alloy containing mainly Ti and iron (Fe) with small amounts of nickel (Ni), vanadium (V), and chromium (Cr). These metal impurities were probably present in the starting materials. The amount of the alloy phase was much less than that of TiC. Both TiC and the metallic alloy were present primarily at the junctions of the TiB_2 grains.

The TiB_2 grains in samples prepared using the B-1 powder (TB9224 and TB9225) were relatively uniform in size, with diameters between 15 and 20 μm, depending on their location in the

compacts. It should be pointed out that almost every line drawn for grain size analysis intercepted some secondary-phase particles. In order to avoid an inaccurate determination of the TiB_2 grain size, the length intercepted by these secondary-phase particles was subtracted from the total length so that the presence of the secondary phase did not alter the TiB_2 grain size measurement.

For TB9246, which was prepared using the B-2 powder, no secondary phases were observed. The average grain size for TB9246 was greater than those for TB9225 and TB9224 (prepared using B-1 powder). This seemed reasonable, considering that the delay time for TB9246 was 20 s, whereas those for TB9224 and TB9225 were 10 and 5 s, respectively. Longer delay times would permit the growth of larger grains. Furthermore, the reaction temperature for TB9246 may also have been higher since the B-2 powder was purer than B-1. This was supported by the observation that the steel rings used for containing the samples prepared using the B-2 powder always showed some signs of melting. In contrast, the steel rings used for the samples prepared using the B-1 powder were intact after the reaction.

5.1.5 Microhardness. The values of Knoop microhardness measured for the three TiB_2 samples were between ≈3,200 and 3,400 kg/mm^2. The hardness values measured on samples from different areas were not significantly different. With such a low load (0.1 kg) and careful selection of locations, indentations were made within TiB_2 grains so that the effect of the grain boundaries on the hardness was greatly reduced. The reported hardness for TiB_2 ranges from 2,710 to 3,900 kg/mm^2, depending on the microstructure of the specimen and test conditions [53]. The hardness given in the literature measured under the same load (0.1 kg) was between 1,800 to 3,500 kg/mm^2. Riley and Niiler [29] reported hardness values between 1,800 and 2,600 kg/mm^2 for SHS/DC TiB_2, and between 2,500 and 3,500 kg/mm^2 for hot-pressed TiB_2. The hardness of TiB_2 measured by Honak [54] under a load of 0.1 kg was 3,400 kg/mm^2. Therefore, the microhardness of the TiB_2 compacts prepared in this research was in excellent agreement with the values reported in the literature. Furthermore, the microhardness of the SHS/DC TiB_2 was comparable to that of the hot-pressed TiB_2.

The effects of test load on the hardness were also examined. The results are shown in Figure 7. When the test load was increased from 0.1 to 5 kg, the measured hardness of TB9225 and TB9224 decreased from 3,300 to 1,200 kg/mm^2. Under a large load, the indentation covered more than 1 grain. The collapse of the grain boundaries resulted in a low value of the measured hardness. This suggested weak grain boundary bonding. The weak grain boundary bonding might have been caused by several factors. First, the individual particles produced by the SHS reaction were randomly oriented. Although the high dynamic pressure could press them into dense body, there was very little atomic-level bonding between grains since the cooling rate was so rapid that the atoms at the grain boundaries did not have an opportunity to adjust themselves. Second, the rapid cooling rate could cause microcracks along the grain boundaries. These microcracks were often observed in the high-magnification micrographs. A microgap is clearly evident along the two neighboring TiB_2 grains in Figure 8.

While the weak grain boundary bonding reduced the macrohardness, it may be beneficial for the fracture toughness since debonding of the grain boundaries can effectively deflect cracks. This is one of the major toughening mechanisms for ceramic materials. The measurement of fracture toughness was not successful because there were usually no major cracks present when Vickers indentations were made on these samples. The effect of grain boundary strength on the hardness and toughness will be addressed during the Phase II effort. Perhaps a relationship between hardness and fracture toughness can be developed.

In order to examine the effect of grain boundary bonding on the hardness, TB9225 was annealed at 1,500 and 2,000° C in Ar for 7.5 hr. Boron nitride crucibles were used. The effect of annealing on the hardness under different loads is shown in Figure 9. Annealing at 1,500° C increased the hardness from about 1,100 to over 1,300 kg/mm^2, whereas annealing at 2,000° C further improved the hardness to 1,550 kg/mm^2. Clearly, the grain boundary strength was improved by annealing, although the improvement was not enough for the grain boundaries to withstand a high load (i.e., 10 kg). Nevertheless, the results are promising and the concept of improving grain boundary strength to produce engineering materials with high bulk hardness was demonstrated.

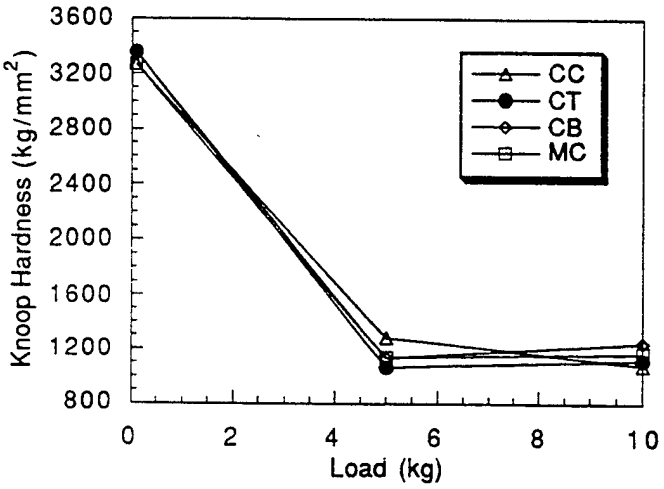

(a) TB9225.

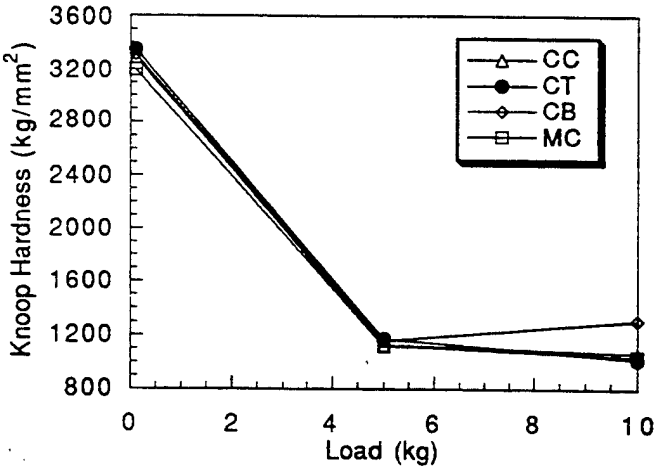

(b) TB9224.

Figure 7. Effect of Test Load on Measured Hardness.

5.1.6 Young's Modulus. The Young's modulus of the TiB_2 samples prepared by the SHS/DC technique was comparable to or greater than that of the hot-pressed TiB_2. The results are presented in Table 3. The average of nine measurements was 548 ± 18 GPa. The Young's modulus for hot-pressed TiB_2, reported by Kotelnikov et al. [55] and Samsonov [56], was 529 GPa.

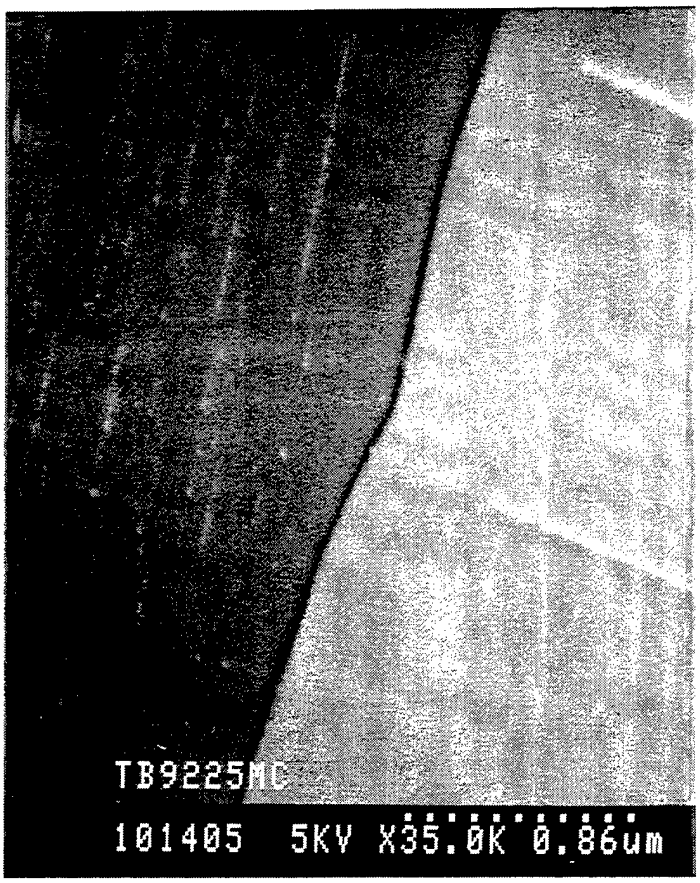

Figure 8. Microcrack Along a Boundary Between Two TiB_2 Grains.

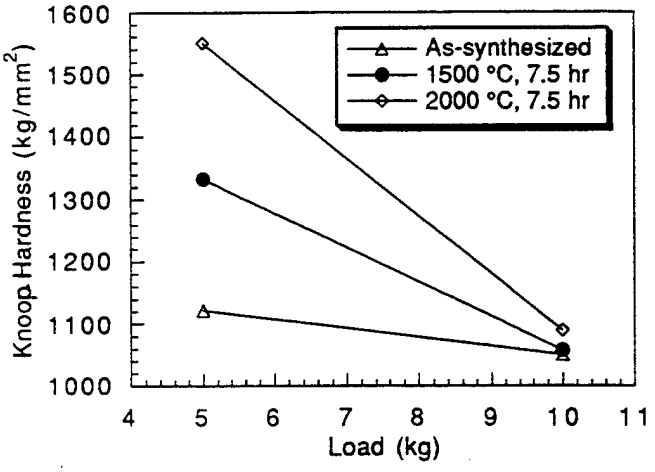

Figure 9. Effect of Annealing Temperature on Hardness of TB9225 Measured Under Different Loads.

5.1.7 Compressive Strength. The compressive strength of the TiB_2 prepared by the present SHS/DC technique was comparable to or in excess of hot-pressed TiB_2. The value presented is the average of three measurements. The compression test was difficult because it required near-perfect alignment of the test system. Any point contacts between the specimen and spacers, or between the spacers and rams, could cause a local failure of the specimen or spacers, resulting in a false measurement. Furthermore, internal defects in the specimens such as cracks could also affect the test results. Therefore, it was expected that the measured compressive strength would vary. The maximum value obtained was 2.51 GPa, while the average was 1.84 GPa. For the sample for which the maximum compressive strength was recorded, failure was accompanied by a loud explosion-like sound, much stronger than that for the other samples. The samples were usually blown into pieces as a result of the sudden release of energy. The compressive strength of hot-pressed TiB_2 measured by Kotelnikov et al. [55] was 1.62 GPa, whereas that reported by Samsonov [56] was 1.32 GPa.

Figure 10 shows a cleavage surface for TB9225 after the compression test. It shows both intergranular and transgranular fracture. It is interesting to note that, during the hardness test, the fracture mode was observed to be predominantly intergranular. The existence of the transgranular fracture in the compression-ruptured samples might be related to the sudden release of the high energy stored in the sample during the test. This, in addition to the fact that the compressive strength of the SHS-prepared TiB_2 was comparable to that of the hot-pressed TiB_2, suggested that the relatively weak grain boundaries did not result in a reduction in the compressive strength.

5.2. TiC.

5.2.1 Physical Appearance of Compacts. As was the case for the TiB_2 compacts, the SHS reacted and explosively compressed TiC compacts were recovered as single piece plates (100 mm in diameter with 25 mm thickness). Photographs of the impact surfaces of TC9223 and TC9242 are shown in Figure 11. The surfaces of the samples were smooth, and the steel rings usually were not distorted. Two types of cracks were observed for the TiC samples: (1) major

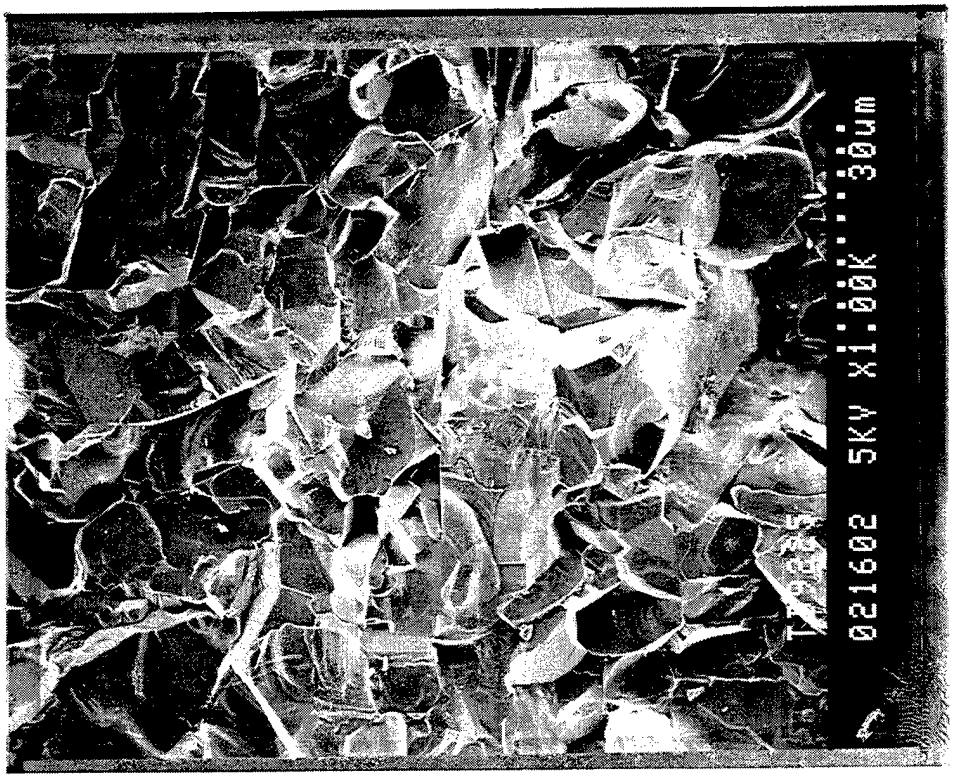

Figure 10. A Cleavage Surface of the Sample TB9225 After the Compression Test. It Shows Both Intergranular and Transgranular Fracture.

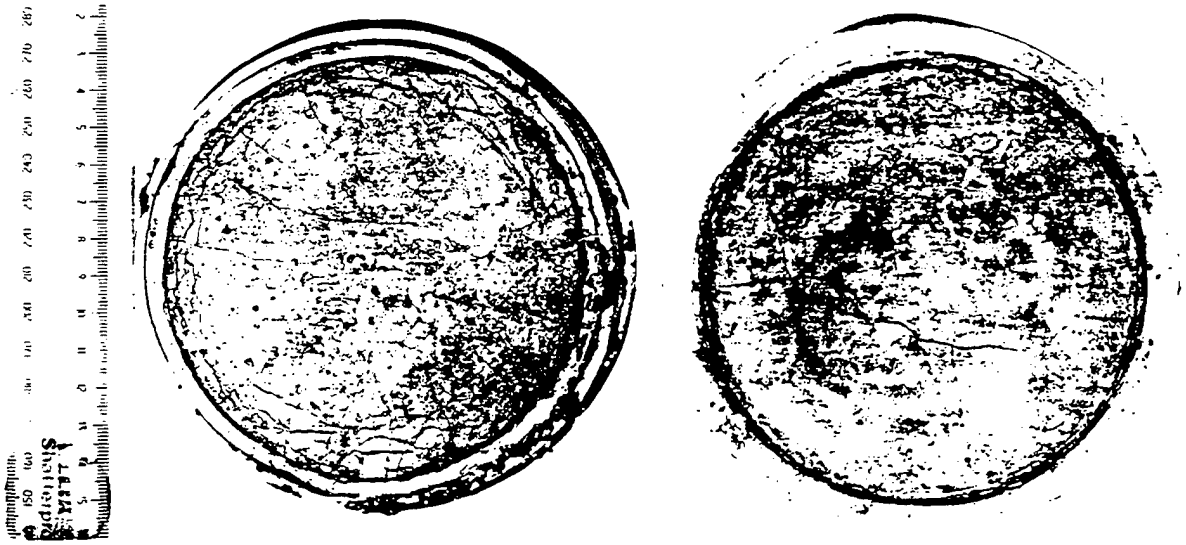

(a) 9223. **(b) 9242.**

Figure 11. Photographs of the Impact Surfaces.

cracks, often going through the samples, and (2) smaller cracks, with a much higher number density. The cracks resulted from residual strains, which may have been caused by the temperature gradients within the compacts during cooling. It is expected that the outer surfaces of the compacts cooled at faster rates than did the cores. Should the residual thermal stresses not be released by plastic deformation, cracks would form as a result. Potential reasons that TiC was more prone to cracking than TiB_2 are its lower heat of reaction and higher thermal expansion coefficient [40].

5.2.2 Density. Samples TC9223 and TC9242 were analyzed for density, composition, grain size, and microhardness. Sample TC9223 was further analyzed to determine its Young's modulus and compressive strength. Some of the results are presented in Table 4. The density was 96.7% of the theoretical density for $TiC_{0.90}$. The target density for TiC in this Phase I project was 95% of the theoretical density.

Table 4. Density, Grain Size, Hardness, Young's Modulus, and Compressive Strength of SHS/DC TiC

Sample	Relative Density (%)	Grain Size[a] (μm)	Hardness[a] (kg/mm^2)	Young's Modulus (GPa)	Compressive Strength (GPa)
TC9223	96.8	CT: 43 ± 16	CT: 2999 ± 202	458 ± 14	1.0 ± 0.2
		CC: 41 ± 14	CC: 2992 ± 356	—	—
		CB: 36 ± 10	CB: 2925 ± 256	—	—
		MC: 35 ± 10	MC: 2985 ± 289	—	—
TC9242	93.7	CT: 36 ± 13	CT: 3012 ± 437	—	—
		CC: 40 ± 13	CC: 2834 ± 303	—	—
		CB: 29 ± 11	CB: 3068 ± 185	—	—
		MC: 34 ± 8	MC: 3005 ± 202	—	—

[a] CT, CC, CB, and MC refer to positions given in Figure 2.

5.2.3 Composition. The XRD pattern of TC9223 is shown in Figure 12. The only phase present was TiC. There was no evidence of residual elemental Ti or C, indicating that the synthesis reaction proceeded to completion. No secondary phases were observed, perhaps due to the use of pure starting materials. Electron probe microanalysis of the TiC grains showed that the C/Ti atomic

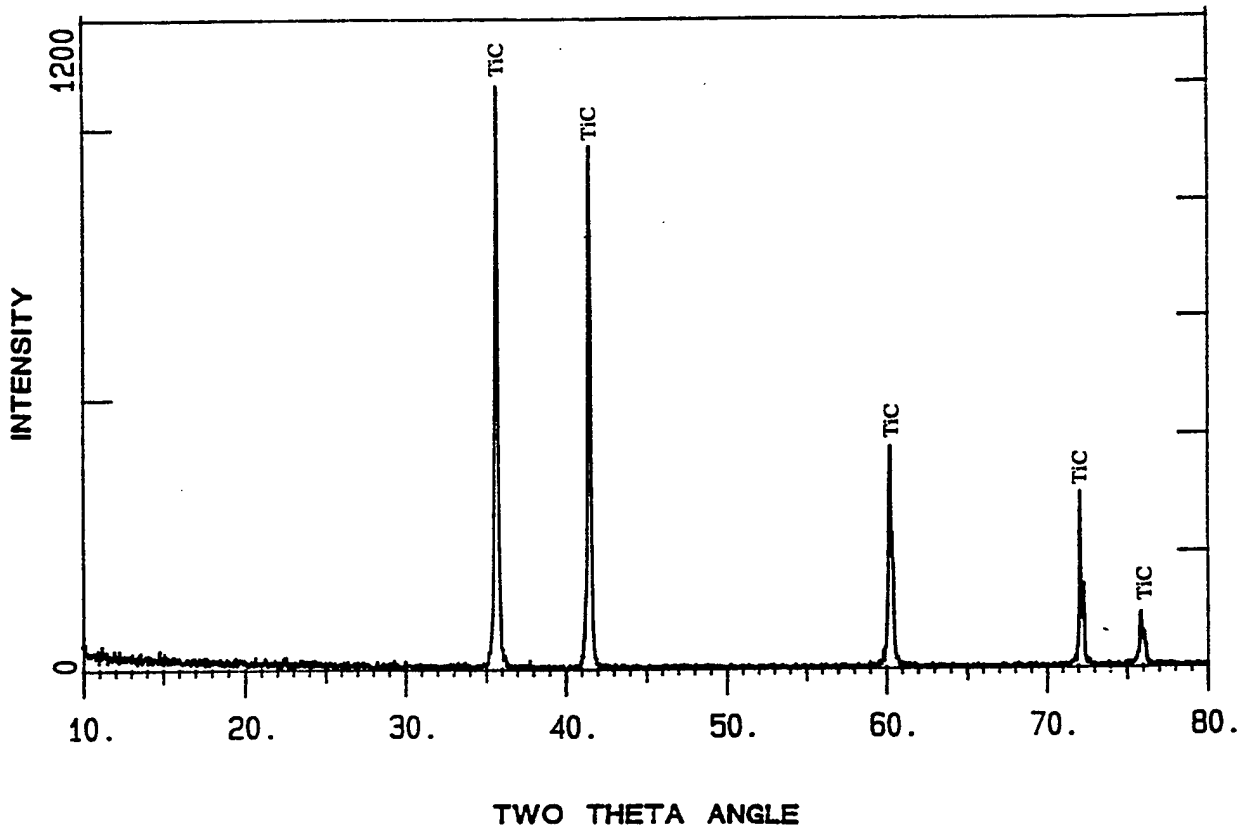

Figure 12. XRD Pattern of TC9223.

ratio was 0.85 ± 0.04. This corresponds to a C atomic fraction of 0.46, which is within the stoichiometric range for TiC, as given in the Ti-C-phase diagram [52].

5.2.4 Microstructure and Grain Size. Figure 13 shows an SEM of TC9223. The TiC grains were more equiaxed than the TiB_2 grains; however, the TiC grains were not of uniform size, as was the case for the TiB_2 samples. The TiC grains in some areas were coarse (≈100 μm), whereas those in other areas were fine (≈20 μm). The average was between 35 and 43 μm. The average grain size in the area close to the impact surface was slightly larger than that in the area close to the nonimpact surface.

Most of large pores (up to several micrometers in diameter) were on the grain boundaries. They were most likely residual pores from the greenform. The small pores (<<1 μm) were

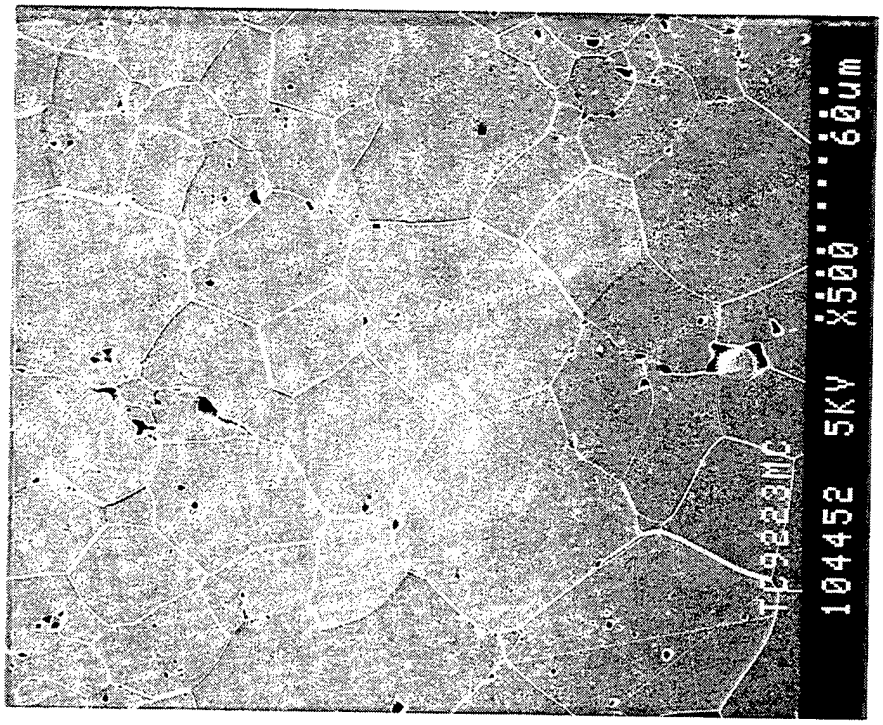

Figure 13. An SEM of TC9223.

predominantly within the TiC grains. They might have resulted from the formation of volatile products during the reaction.

5.2.5 Microhardness. The Knoop microhardness values of TC9223 and TC9242 were approximately 3,000 kg/mm^2. As was the case for the TiB_2 samples, the hardness measured for the TiC sample from different areas was similar. The microhardness measured for the present TiCcompacts was generally in agreement with those reported in the literature. More importantly, the microhardness of the SHS/DC TiC was comparable to that of the hot-pressed TiC. The reported hardness for TiC ranges from 1,500 to 3,200 kg/mm^2. The hardness reported by Kieffer and Kölbl [57], for the same load used in this research (0.1 kg), was 3,200 kg/mm^2. Riley and Niiler [29] reported values between 1,500 and 2,700 kg/mm^2 for SHS/DC TiC, and between 2,400 and 3,100 kg/mm^2 for hot-pressed TiC. The discrepancy between reported values has been attributed to differences in the microstructures of the specimens and/or the test conditions [5].

The effects of test load on the hardness were also examined for TC9223 and TC9242. The results are shown in Figure 14. The hardness decreased from 3,000 to 1,500 kg/mm^2, as the test load was increased from 0.1 to 5 kg. Further increases in the load did not result in a significant

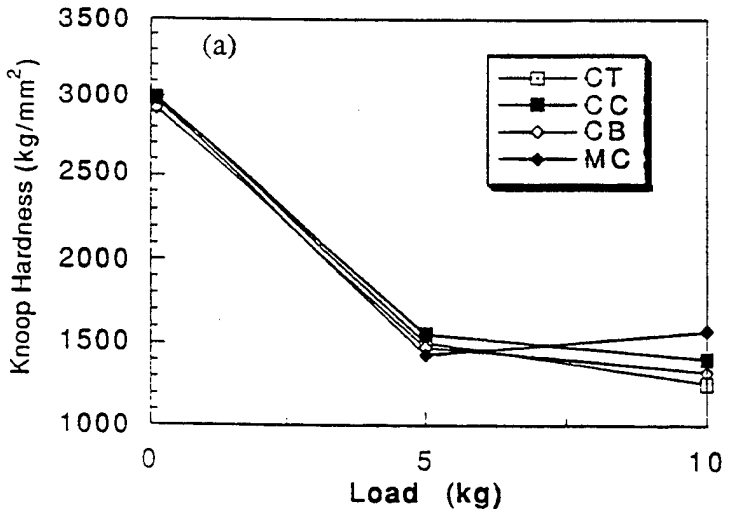

(a) TC9223.

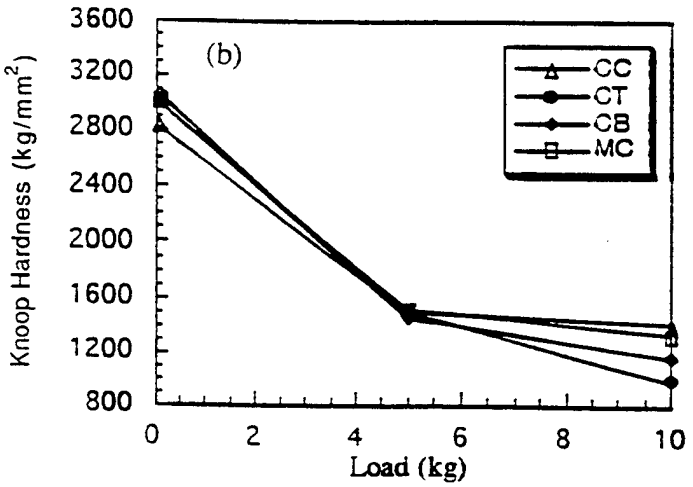

(b) TC9242

Figure 14. Effects of Test Load on the Hardness of TiC Samples.

further reduction in the hardness. This reduction in hardness with test load was related to weak grain boundaries; however, it was noticed that the decrease in hardness with test load was less dramatic for TiC than for TiB_2. The hardness of TiB_2 measured under a test load of 5 kg was only 1,200 kg/mm^2, whereas that for TiC was 1,500 kg/mm^2. Note that the hardness of TiB_2 measured under a load of 0.1 kg was higher (≈3,400 kg/mm^2) than that of TiC (≈3,000 kg/mm^2). These results suggest that the grain boundary strength in TiC was greater than that in TiB_2 and that TiC might be superior to TiB_2 for some hardness applications.

The sample TC9223 was annealed at 1,500 and 2,000° C for 7.5 hr in an Ar atmosphere to examine the effect of grain boundary strength on the hardness measured under different loads. The result is shown in Figure 15. Annealing at 1,500° C did not increase the hardness (the exceptional data point under a test load of 10 kg might be due to the nonuniformity of the TiC microstructure). Annealing at 2,000° C for 7.5 hr significantly increased the hardness measured under a test load of 5 kg but did not increase the hardness measured under a test load of 10 kg. The less dramatic effect of annealing on the hardness of TiC compared to TiB_2 might be due to the higher melting temperature of TiC and the stronger initial grain boundary bonding for TiC.

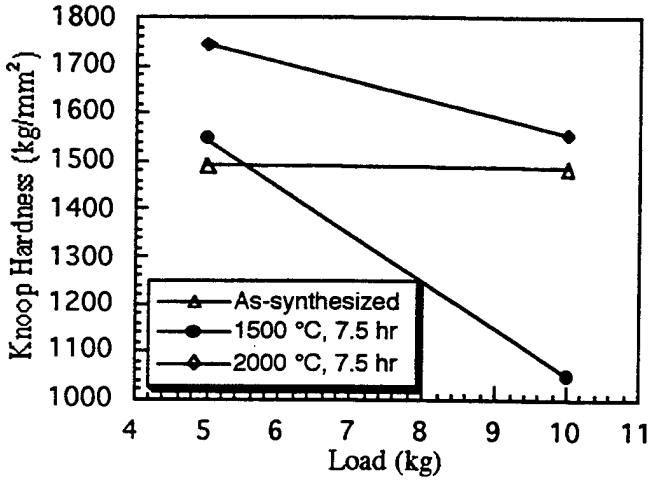

Figure 15. Effect of Annealing Temperature on the Hardness of TC9223 Under Different Loads.

5.2.6 Young's Modulus. The Young's modulus of TiC prepared by SHS/DC was 548 ± 14. This value is the average of seven measurements. The elastic moduli reported by Samsonov [58], were 451 GPa; that by McMurtry et al. [59] were 531 GPa; and that by Kingery, Bowen, and Uhlmann [60] were 310 GPa. The present result was in good agreement with the Young's modulus reported by Samsonov.

5.2.7 Compressive Strength. The compressive strength of TiC was 1.0 ± 0.2 GPa (average of three measurements). The measured compressive strength was lower than the value reported by Samsonov (1.35 GPa) [58]. This might be due to the extensive cracks present in our TiC

samples. The cracks could cause local failures in the samples, resulting in lower compressive strengths. Figure 16 is a cleavage surface of the sample TC9223 after the compression test. Similar to observations for TB9225, a mode including both intergranular and transgranular fractures was observed for TC9223. The transgranular fracture might be due to the sudden release of strain energy stored in the sample.

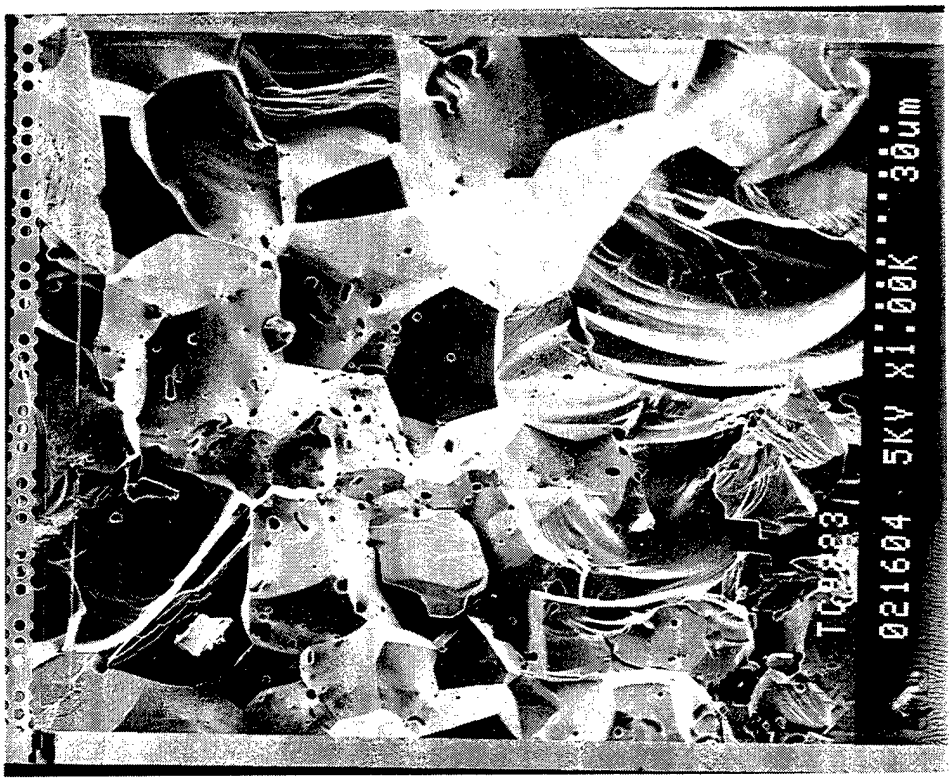

Figure 16. A Cleavage Surface of TC9223 After the Compression Test.

6. Summary

The primary objective of this Phase I effort was to produce plates of TiB_2 at 98% of theoretical density and TiC at 95% of theoretical density using the SHS and DC technique. The compositional, microstructural, and mechanical properties of these materials were evaluated.

TiB_2 and TiC compacts with diameters of 100 mm and thicknesses of 25 mm were fabricated successfully. Theoretical densities of 99% for TiB_2 and almost 97% for TiC were achieved, thus satisfying the primary goal of this research. The hardnesses measured using a load of 0.1 kg for SHS/DC TiB_2 and TiC averaged 3,286 and 2,975 kg/mm^2 (32.2 and 29.2 GPa), respectively. The hardness decreased as the applied load was increased, indicating that the grain boundaries were relatively weak. Annealing in Ar at temperatures greater than or equal to 1,500° C increased the hardness measured at a load of 5 kg. The Young's moduli were 548 GPa for TiB_2 and 458 GPa for TiC, and the compressive strengths were 1.8 GPa for TiB_2 and 1.0 GPa for TiC. The mechanical properties of these SHS/DC ceramics were comparable to or greater than those reported for materials prepared by conventional hot-pressing methods.

It was found that the TiB_2 plates prepared using the less-pure B powders (1–5% C impurity) had mechanical properties comparable to those of plates prepared using the pure powders. According to projections by Niiler et al. [30], the raw materials costs could account for 66% of the total production cost for SHS/DC TiB_2 and about 23% for SHS/DC TiC, if pure precursors are employed. If, as indicated by the present experimental results, high-quality TiB_2 and TiC plates can be produced from less-pure powders or mixtures of B and C without sacrificing the density and/or mechanical properties, the total production costs could be greatly reduced.

7. References

1. Wilkins, M. L. "2nd Progress Report of Light Armor Program." UCRL-50349, Lawrence Radiative Laboratory, University of California, Livermore, CA, 1976.

2. Wilkins, M. L., R. L. Landingham, and C. A. Honodel. "5th Progress Report of Light Armor Program. UCRL-50349, Lawrence Radiative Laboratory, University of California, Livermore, CA, 1976.

3. Samsonov, G. V., and B. A. Kovenskaya. *Boron and Refractory Borides.* P. 5, V. I. Matkovich (editor), Berlin, Germany: Springer-Verlag, 1977.

4. Toth, L. E. *Transition Metal Carbides and Nitrides.* New York, NY: Academic Press, 1971.

5. Storms, E. K. *The Refractory Carbides.* New York, NY: Academic Press. 1967.

6. Yamada, O., Y. Maimed, and M. Koizumi. "High Pressure Self-Combustion Sintering of Silicon Carbide." *American Ceramic Society Bulletin*, vol. 64, no. 2, pp. 319–321, 1985.

7. Holt, J. B., D. D. Kingman, and G. M. Bianchini. "Kinetics of Combustion Synthesis of TiB_2." *Materials Science and Engineering,* vol. 71, pp. 321–327, 1985.

8. Rice, R. W., and W. J. McDonough. "Intrinsic Volume Changes of Self-Propagating Synthesis." *Journal of American Ceramic Society*, vol. 68, no. 5, pp. C122–C123, 1985.

9. Holt J. B., and Z. A. Munir. "Combustion Synthesis of Titanium Carbide: Theory and Experiment." *Journal of Materials Science*, vol. 21, no. 1, pp. 251–259, 1986.

10. Hirao, K., Y. Maimed, and M. Koizumi. "Sintering of Si_3N_4 Powders Synthesized by a Combustion Reaction." *Yogyo Kyokai Shi*, vol. 95, no. 10, pp. 955–960, 1987.

11. Munir, Z. A. "Synthesis of High Temperature Materials by Self-Propagating Combustion Methods." *American Ceramic Society Bulletin*, vol. 67, no. 2, pp. 342–348, 1988.

12. Dunmead, S. D., D. W. Ready, and C. E. Semler. "Kinetics of Combustion Synthesis in the Ti-C and Ti-C-Ni Systems." *Journal of American Ceramic Society*, vol. 72, no. 12, pp. 2318–2324, 1989.

13. Munir, Z. A., and U. Anselmi-Tamburini. "Self-Propagating Exothermic Reactions: The Synthesis of High Temperature Materials by Combustion." *Materials Science Report*, vol. 3, no. 7–8, pp. 277–365, 1989.

14. Choi, Y., M. E. Mullins, K. Wijayatilleke, and J. K. Lee. "Processing Effects on the Morphology of Titanium Carbide in Self-Propagating High-Temperature Synthesis." *High Temperature Technology*, vol. 8, no. 3, pp. 227–229, 1990.

15. Trambukis, J., and Z. A. Munir. "Effect of Particle Dispersion on the Mechanism of Combustion Synthesis of Titanium Silicide." *Journal of the American Ceramic Society*, vol. 73, no. 5, pp. 1240–1245, 1990.

16. Eslamloo-Grami, M., and Z. A. Munir. "Effect of Porosity on the Combustion Synthesis of Titanium Nitride." *Journal of the American Ceramic Society*, vol. 73, no. 5, pp. 1235–1239, 1990.

17. Agrafiotis, C. C., J. Lis, J. A. Puszynski, and V. Hlavacek. "Combustion Synthesis of Silicon Nitride-Silicon Carbide Composites." *Journal of the American Ceramic Society*, vol. 73, no. 11, pp. 3514–3517, 1990.

18. Yi, H. C., and J. J. Moore. "Self-Propagating High-Temperature Combustion Synthesis (SHS) of Powder-Compacted Materials." *Journal of Materials Science*, vol. 25, no. 2B, pp. 1159–1168, 1990.

19. Deevi, S. C. "Structure of the Combustion Wave in the Combustion Synthesis of Titanium Carbide." *Journal of Materials Science*, vol. 26, no. 10, pp. 2662–2670, 1991.

20. Rice, R. W. "Microstructural Aspects of Fabricating Bodies by Self-Propagating Synthesis." *Journal of Materials Science*, vol. 26, no. 24, pp. 6533–6541, 1991.

21. Zeng, J., Y. Maimed, and O. Yamada. "Combustion Synthesis of Si_3N_4-SiC Compisite Powders." *Journal of the American Ceramic Society*, vol. 74, no. 9, pp. 2197–2200, 1991.

22. Richardson, G. Y., R. W. Rice, W. J. McDonough, J. M. Kunetz, and T. Schroeter. "Hot Pressing of Ceramics Using Self-Propagating Synthesis. "*Ceramic Engineering and Science Proceedings*, vol. 7, no. 7–8, pp. 761–770, 1985.

23. Zavitsanos, P. D., J. J. Gebhardt, and A. Gatti. "The Use of Self-Propagating High-Temperature Synthesis of High-Density Titanium Diboride." *Combustion and Plasma Synthesis of High Temperature Materials*, pp. 170–178, Z. A. Munir and J. B. Holt (editors), New York, NY: VCH Publishers, 1990.

24. Miyamoto, Y. "New Ceramic Processing Approaches Using Combustion Synthesis Under Gas Pressure." *American Ceramic Society Bulletin*, vol. 69, no. 4, pp. 686–690, 1990.

25. Hirao, K., Y. Miyamoto, and M. Koizumi. "Synthesis of Silicon Nitride by a Combustion Reaction Under High Nitrogen Pressure." *Journal of the American Ceramic Society*, vol. 69, no. 4, pp. C60–C61, 1986.

26. Vecchio, K., J. C. LaSalvia, M. A. Meyers, and G. T. Gray, III. "Microstructural Characterization of Self-Propagating High-Temperature Synthesis/Dynamically Compacted and Hot-pressed Titanium Carbides." *Metallurgical Transactions A*, vol. 23A, no. 1, pp. 87–97, 1992.

27. LaSalvia, J. C., L. W. Meyer, and M. A. Meyers. "Densification of Reaction-Synthesized Titanium Carbide by High-Velocity Forging." *Journal of the American Ceramic Society*, vol. 75, no. 3, pp. 592–602, 1992.

28. Rice, R. W., W. J. McDonough, G. Y. Richardson, J. M. Kunetz, and T. Schroeter, "Hot Rolling of Ceramics Using Self-Propagating High-Temperature Synthesis." *Ceramic Engineering and Science Proceedings*, vol. 7, no. 7–8, pp. 751–760, 1985.

29. Riley, M. A., and A. Niiler. "Low Pressure Compaction of SHS (Self-Propagating High-Temperature Synthesis) Prepared Ceramics." BRL-MR-3574, U.S. Army Ballistic Research Laboratory, Aberdeen Proving Ground, MD, 1987.

30. Niiler, A., L. J. Kecskes, T. Kottke, P. H. Netherwood, Jr., and R. F. Benck, "Explosive Consolidation of Combustion Synthesized Ceramics: Titanium Carbide (TiC) and Titanium Diboride (TiB_2)." BRL-TR-2951, U.S. Army Ballistic Research Laboratory, Aberdeen Proving Ground, MD, 1988.

31. Niiler, A., L. J. Kecskes, and T. Kottke. "Shock Consolidation of Combustion-Synthesized Ceramics." *Combustion of Plasma Synthesis of High Temperature Materials*, pp. 309–314, Z. A. Munir and J. B. Holt (editors), New York, NY: VCH Publishers, 1990.

32. Grebe, H. A. Private communication. New Mexico Institute of Mining and Technology, Socorro, NM, 1991.

33. Kottke, T., L. J. Kecskes, and A. Niiler. "Control of Titanium Diboride SHS Reactions by Inert Dilutions and Mechanical Constraint." *American Institute of Chemical Engineers Journal,* vol. 36, no. 10, pp. 1581–1584, 1990.

34. Kecskes L. J., and A. Niiler. "Impurities in the Combustion Synthesis of Titanium Carbide." *Journal of the American Ceramic Society*, vol. 72, no. 4, pp. 655–661, 1989.

35. Kecskes, L. J., T. Kottke, and A. Niiler. "Microstructural Properties of Combustion-Synthesized and Dynamically-Consolidated Titanium Boride and Titanium Carbide." *Journal of the American Ceramic Society,* vol. 73, no. 5, pp. 1274–1282, 1990.

36. Kottke, T., L., J. Kecskes, and A. Niiler. "Combustion Synthesis Dynamics Modeling." *Combustion and Plasma Synthesis of High Temperature Materials*, p. 238, Z. A. Munir and J. B. Holt (editors), VCH, NY, 1990.

37. Kecskes, L. J., R. F. Benck, and P. H. Netherwood. "Dynamic Compaction of Combustion Synthesized Hafnium Carbide." *Journal of the American Ceramic Society*, vol. 73, no. 2, pp. 383–387, 1990.

38. Merzhanov, A. G. and I. P. Borovinskaya. "Self-Propagating High-Temperature Synthesis of Refractory Inorganic Compounds." *Doklady Chemistry*, vol. 204, no. 2, pp. 429–432, 1972.

39. Crider, J. F. "Self-Propagating High Temperature Synthesis - A Soviet Method for Producing Ceramic Materials." *Ceramic Engineering Science Proceedings*, vol. 3, no. 9–10, pp. 519–537, 1982.

40. Grebe, H. A. "High-Rate Chemical Reaction and Dynamic High-Pressure Processing of Titanium Carbide Ceramics." Ph.D. Thesis, New Mexico Institute of Mining and Technology, Socorro, NM, 1996.

41. Cutler R. A., A. V. Virkar, and J. B. Holt. "Synthesis and Densification of Oxide-Carbide Composites." *Ceramic Engineering and Science Proceedings*, vol. 6, no. 7–8, pp. 715–728, 1985.

42. McCauley, J. W., N. D. Corbin, T. M. Resetar, and P. Wong. "Simultaneous Preparation and Self-Sintering of Materials in the Titanium-Boron-Carbon System." *Ceramic Engineering and Science Proceedings*, vol. 3, no. 9–10, pp. 504–511, 1982.

43. Advani, A. H., N. N. Thadhani, H. A. Grebe, R. Heaps, C. Coffin, and T. Kottke. "Dynamic Modelling of Material and Process Parameter Effects on Self-Propagating High-Temperature Synthesis of Titanium Carbide Ceramics." *Journal of Materials Science*, vol. 27, no. 12, pp. 3309–3317, 1992.

44. Advani, A. H. Private communication. University of Texas at El Paso, El Paso, TX, 1991.

45. Yamada, O., Y. Maimed, and M. Koizumi. "High-Pressure Self-Combustion Sintering of Titanium Carbide." *Journal of the American Ceramic Society*, vol. 70, no. 9, pp. C206-C208, 1987.

46. Miracle, D. B., and H. A. Lipsitt. "Mechanical Properties of Fine-grained Substoichiometric Titanium Carbide." *Journal of the American Ceramic Society*, vol. 66, no. 8, pp. 592–597, 1983.

47. U.S. Army Research Laboratory. "Armor, Plate, Steel, Wrought, High-Hardness." Weapons and Materials Research Directorate, Aberdeen Proving Ground, MD, 29 June 1990.

48. Ramberg, J. R., and W. S. Williams. "High Temperature Deformation of Titanium Diboride." *Journal of Materials Science*, vol. 22, no. 5, pp. 1815–1826, 1987.

49. Castellan, G. W. *Physical Chemistry*. Reading, MA: Addison-Wesley, 1971.

50. Mendelson, M. I. "Average Grain Size in Polycrystalline Ceramics." *Journal of the American Ceramic Society*, vol. 52, no. 8, pp. 443–446, 1969.

51. Kittel, C. *Introduction to Solid State Physics*. New York, NY: John Wiley Sons, 1953.

52. Massalski, T. B., (editor-in chief). *Binary Alloy Phase Diagrams*. Vol. 1. Metals Park, OH: American Society for Metals, 1986.

53. McColm, I. J. *Ceramic Hardness*. New York, NY: Plenum Press, 1990.

54. Honak, E. R. "Ueber Hochschmelzende Boride der Uebergangsmetalle und ein Neues Darstellungsverfahren von Titan- und Zirkondiborid." Thesis, Technische Hochschule, Graz, Austria, 1951.

55. Kotelnikov, R. B., N. Bashlykov, Z. G. Galiachbarov, and A. J. Kashtanov. *Especially High Melting Elements and Compounds*. Isdatel'stvo Metallurgija, Moscow, 1969.

56. Samsonov, G. V. *Refractory Compounds*. Moscow, Russia: Mettalurgizdat, 1963.

57. Kieffer, R. and F. Kölbl. *Powder Metallurgy Bulletin*. Vol. 4, no. 1, pp. 4–17, Tungsten Carbide-Free Hard Metals, 1949.

58. Samsonov, G. V. *Plenum Press Handbook of High-Temperature Materials No. 2 Properties Index*. New York, NY: Plenum Press 1962.

59. McMurtry, C. H., W. D. G. Boecker, S. G. Seshadri, J. S. Zanghi, and J. E. Garnier. "Microstructure and Material Properties of SiC-TiB_2." *American Ceramic Society Bulletin*, vol. 66, no. 2, pp. 325–329, 1987.

60. Kingery, W. D., H. K. Bowen, and D. R. Uhlmann. *Introduction to Ceramics*. New York, NY: John Wiley Sons, 1976.

INTENTIONALLY LEFT BLANK.

NO. OF COPIES ORGANIZATION

2 DEFENSE TECHNICAL INFORMATION CENTER
DTIC DDA
8725 JOHN J KINGMAN RD
STE 0944
FT BELVOIR VA 22060-6218

1 HQDA
DAMO FDQ
D SCHMIDT
400 ARMY PENTAGON
WASHINGTON DC 20310-0460

1 OSD
OUSD(A&T)/ODDDR&E(R)
R J TREW
THE PENTAGON
WASHINGTON DC 20301-7100

1 DPTY CG FOR RDE HQ
US ARMY MATERIEL CMD
AMCRD
MG CALDWELL
5001 EISENHOWER AVE
ALEXANDRIA VA 22333-0001

1 INST FOR ADVNCD TCHNLGY
THE UNIV OF TEXAS AT AUSTIN
PO BOX 202797
AUSTIN TX 78720-2797

1 DARPA
B KASPAR
3701 N FAIRFAX DR
ARLINGTON VA 22203-1714

1 NAVAL SURFACE WARFARE CTR
CODE B07 J PENNELLA
17320 DAHLGREN RD
BLDG 1470 RM 1101
DAHLGREN VA 22448-5100

1 US MILITARY ACADEMY
MATH SCI CTR OF EXCELLENCE
DEPT OF MATHEMATICAL SCI
MAJ M D PHILLIPS
THAYER HALL
WEST POINT NY 10996-1786

NO. OF COPIES ORGANIZATION

1 DIRECTOR
US ARMY RESEARCH LAB
AMSRL D
R W WHALIN
2800 POWDER MILL RD
ADELPHI MD 20783-1145

1 DIRECTOR
US ARMY RESEARCH LAB
AMSRL DD
J J ROCCHIO
2800 POWDER MILL RD
ADELPHI MD 20783-1145

1 DIRECTOR
US ARMY RESEARCH LAB
AMSRL CS AS (RECORDS MGMT)
2800 POWDER MILL RD
ADELPHI MD 20783-1145

3 DIRECTOR
US ARMY RESEARCH LAB
AMSRL CI LL
2800 POWDER MILL RD
ADELPHI MD 20783-1145

ABERDEEN PROVING GROUND

4 DIR USARL
AMSRL CI LP (305)

NO. OF COPIES	ORGANIZATION
2	US ARMY ARDEC D KAPOOR S CYTRON DOVER NJ 07801
3	ARMY RSRCH OFFICE A CROWSON E CHEN R REEBER PO BOX 12211 RSRCH TRIANGLE PRK NC 22709-2211
1	BATTELLE PACIFIC NW LABORATORIES W GURWELL PO BOX 999 RICHLAND WA 99352
1	PENNSYLVANIA STATE UNIV DEPT ENGNR SCIENCES AND MECHANICS R GERMAN 227 HAMMOND BLDG UNIVERSITY PARK PA 16802-1401
1	UNIV OF CALIFORNIA SAN DIEGO DEPT APPLIED MECHANICS AND ENGNR SCIENCES M MEYERS MAIL CODE 0411 9500 GILMAN DRIVE LA JOLLA CA 92093-0411
2	GEORGIA INST OF TECH SCHL OF MTRL ENG K LOGAN N THADHANI ATLANTA GA 30332-0245
3	NEW MEXICO INST OF MINING AND TECH CTR FOR EXPLSV TECH AND RSRCH A MILLER P PERSSON MTRLS AND MET ENG O INAL SOCORRO NM 87801

NO. OF COPIES	ORGANIZATION
1	UNIV OF CALIFORNIA COLLEGE OF ENGNRNG Z MUNIR DAVIS CA 95616
	ABERDEEN PROVING GROUND
30	USARL AMSRL WM TE L KECSKES (15 CPS) A NIILER AMSRL WM TA W GOOCH W GILLICH M BURKINS G HAUVER T HAVEL E HORWATH AMSRL WM TD K FRANK AMSRL WM TC E KENNEDY L MAGNESS AMSRL WM MC J LASALVIA T HYNES J MCCAULEY D VIECHNICKI J WELLS

REPORT DOCUMENTATION PAGE

Form Approved
OMB No. 0704-0188

1. AGENCY USE ONLY *(Leave blank)*	2. REPORT DATE	3. REPORT TYPE AND DATES COVERED
	April 1999	Final, 13 May - 14 Dec 91

4. TITLE AND SUBTITLE
Self-Propagating High-Temperature Synthesis and Dynamic Compaction of Titanium Boride and Titanium Carbide

5. FUNDING NUMBERS
C: DAAA 15-91-C-0088

6. AUTHOR(S)
Liya Wang and Levi T. Thompson

7. PERFORMING ORGANIZATION NAME(S) AND ADDRESS(ES)
T/J Technologies, Inc.
3850 Research Park Drive
PO Box 2150
Ann Arbor, MI 48106

8. PERFORMING ORGANIZATION REPORT NUMBER

9. SPONSORING/MONITORING AGENCY NAMES(S) AND ADDRESS(ES)
U.S. Army Research Laboratory
ATTN: AMSRL-WM-TE
Aberdeen Proving Ground, MD 21005-5066

10.SPONSORING/MONITORING AGENCY REPORT NUMBER
ARL-CR-440

11. SUPPLEMENTARY NOTES
Point of contact for this report is Dr. Laszlo Kecskes, U.S. Army Research Laboratory, ATTN: AMSRL-WM-TE, Aberdeen Proving Ground, MD 21005-5066.

12a. DISTRIBUTION/AVAILABILITY STATEMENT
Approved for public release; distribution is unilimited.

12b. DISTRIBUTION CODE

13. ABSTRACT *(Maximum 200 words)*

Titanium carbide (TiC) and titanium diboride (TiB_2) ceramic disks, with diameters of 100 mm and thicknesses of 25 mm were fabricated with densities above 95% and 98% of theoretical, respectively, using a self-propagating high-temperature synthesis/dynamic consolidation (SHS/DC) process. First, an SHS reaction was initiated in a green body made from precursor powders. Second, after the completion of the SHS reaction, the freshly synthesized ceramic product was densified to near-full density by the action of the detonation of an explosive. With a focus on potential military and civilian applications, the structural and mechanical properties of the products were evaluated. Furthermore, the relationship between process conditions, microstructure development, and mechanical properties was investigated. Finally, correlations of the properties with key processing conditions were used to establish guidelines for the fabrication, scale-up, and commercialization of the process.

14. SUBJECT TERMS
titanium, carbon, boron, titanium carbide, titanium diboride, SHS, DC, explosive compaction

15. NUMBER OF PAGES
44

16. PRICE CODE

17. SECURITY CLASSIFICATION OF REPORT	18. SECURITY CLASSIFICATION OF THIS PAGE	19. SECURITY CLASSIFICATION OF ABSTRACT	20. LIMITATION OF ABSTRACT
UNCLASSIFIED	UNCLASSIFIED	UNCLASSIFIED	UL

INTENTIONALLY LEFT BLANK.

USER EVALUATION SHEET/CHANGE OF ADDRESS

This Laboratory undertakes a continuing effort to improve the quality of the reports it publishes. Your comments/answers to the items/questions below will aid us in our efforts.

1. ARL Report Number/Author ARL-CR-440 (Wang [POC: Kecskes]) Date of Report April 1999

2. Date Report Received _____

3. Does this report satisfy a need? (Comment on purpose, related project, or other area of interest for which the report will be used.) _____

4. Specifically, how is the report being used? (Information source, design data, procedure, source of ideas, etc.) _____

5. Has the information in this report led to any quantitative savings as far as man-hours or dollars saved, operating costs avoided, or efficiencies achieved, etc? If so, please elaborate. _____

6. General Comments. What do you think should be changed to improve future reports? (Indicate changes to organization, technical content, format, etc.) _____

CURRENT ADDRESS

_____
Organization

_____
Name E-mail Name

_____
Street or P.O. Box No.

_____
City, State, Zip Code

7. If indicating a Change of Address or Address Correction, please provide the Current or Correct address above and the Old or Incorrect address below.

OLD ADDRESS

_____
Organization

_____
Name

_____
Street or P.O. Box No.

_____
City, State, Zip Code

(Remove this sheet, fold as indicated, tape closed, and mail.)

(DO NOT STAPLE)